

Raman and ultrafast optical spectroscopy of acoustic phonons in $\text{CdTe}_{0.68}\text{Se}_{0.32}$ quantum dots

A. V. Bragas,^{1,2,*} Cynthia Aku-Leh,^{2,†} and Roberto Merlin²

¹*Departamento de Física, FCEyN, Universidad de Buenos Aires, 1428 Buenos Aires, Argentina*

²*FOCUS Center and Department of Physics, The University of Michigan, Ann Arbor, Michigan 48109-1040, USA*

(Received 11 December 2005; published 7 March 2006)

Acousticlike vibrations were observed in spontaneous Raman measurements on $\text{CdTe}_{0.68}\text{Se}_{0.32}$ quantum dots embedded in a borosilicate matrix and ascribed to the $l=0$, $l=2$, and $l=1$ modes of a spherical particle. Pump-probe stimulated Raman measurements on the same sample reveal only the symmetric $l=0$ mode, the frequency of which increases as the laser central energy moves to higher energies. Consistent with the strong dependence of the exciton energy on the particle size, such a behavior is attributed to resonant size-selective excitation of nanocrystallites whose absorption edge coincides with the central energy of the optical pulses. This selectivity, relying on the existence of double-resonant terms in the generation process, is not observed in spontaneous Raman scattering for which the resonances involve a single term.

DOI: [10.1103/PhysRevB.73.125305](https://doi.org/10.1103/PhysRevB.73.125305)

PACS number(s): 78.47.+p, 78.30.-j, 42.65.Dr, 63.22.+m

I. INTRODUCTION

Semiconductor nanocrystals or quantum dots (QDs) have been extensively studied in the past several decades due to the applications they offer as well as the basic research interest of the physics and chemistry communities on low-dimensional systems. In particular, QDs are beginning to receive acceptance as molecular labels in biological applications where they may replace dye molecules.^{1,2} Semiconductor doped glasses have long attracted attention for potential uses in optoelectronics. Since the glass matrix is transparent in the visible range, the optical properties of these composite materials are determined by those of the QDs. Because the emission of phonons is one of the most important electronic dephasing mechanisms, there has been much interest in the vibrational properties of QDs. Optical phonons,^{3–5} confined acoustic phonons,^{4,6–9} and surface^{10,11} and disorder-activated phonons^{12,13} in semiconductor nanocrystallites have been extensively investigated with spontaneous Raman scattering (RS). The propagation of subpicosecond laser pulses generally leads to the production of coherent phonon fields, the amplitude of which is resonantly enhanced when the laser central energy is tuned near an electronic resonance.¹⁴ The study of coherent phonons in semiconductor QDs, driven by ultrafast pulsed lasers, is relatively a new field. Coherent techniques allow direct time-domain observation as well as active control of vibrational modes and, as such, they offer new possibilities for studying ultrafast phonon dynamics.

In this paper we report on the impulsive generation of acoustic phonons in $\text{CdTe}_{0.68}\text{Se}_{0.32}$ nanocrystallites. We generate coherent oscillations by impulsive stimulated Raman scattering (SRS) using a standard pump-probe setup with ultrafast laser pulses tuned to the absorption edge of the QDs. We also report on RS measurements performed on the same sample and excitation range, and compare these results with those of the SRS measurements. The first observation of coherent acoustic phonons in QDs was reported by Krauss and Wise¹⁵ for PbS. These authors noticed an intriguing discrepancy between spontaneous Raman and pump-probe results in that the Raman spectra reveal an extra mode.

Ikezawa *et al.*¹⁶ reported similar results for PbSe QDs. We have also found striking differences between Raman and pump-probe spectra in $\text{CdTe}_{0.68}\text{Se}_{0.32}$. In particular, we find that the frequency of a fully symmetric acoustic mode exhibits a strong dependence on the laser energy in the pump probe, but not in the RS data. The time-domain observations are ascribed to size selectivity within the distribution of dots, an effect which, we believe, relies on double-resonant terms which operate for pump-probe excitation but not for spontaneous RS. The observed size selectivity offers interesting possibilities for partially removing effects due to inhomogeneous broadening.

II. EXPERIMENTAL

Our sample is a commercial 3-mm-thick RG780 filter (Schott Glass Technologies, Inc.) made of semiconductor nanocrystallites of $\text{CdTe}_{0.68}\text{Se}_{0.32}$ embedded in a borosilicate matrix.³ Bulk $\text{CdTe}_{1-x}\text{Se}_x$ crystallizes in the zincblende structure for $x < 0.36$.^{17,18} The energy bandgap E_g versus composition exhibits bowing. At $x=0.32$, $E_g=1.4$ eV. The electronic and hole spatial confinement in the dots produces a blue-shift of the gap, which can be determined by measuring the sample transmission, shown in Fig. 1(a). As in our previous work on optical phonons,¹⁴ we use these results to obtain the first excitonic transition, $E_1=1.68$ eV, and the average radius of the sample, $a=39$ Å.

Bulk $\text{CdTe}_{1-x}\text{Se}_x$ shows two-mode phonon behavior leading to two, each, CdSe-like and CdTe-like longitudinal optical (LO) and transverse optical (TO) phonons. The frequencies of these phonons vary with the alloy composition. For $x=0.32$, these are, approximately, 190 cm^{-1} (LO) and 170 cm^{-1} (TO) for the CdSe-like, and 160 cm^{-1} (LO) and 140 cm^{-1} (TO) for the CdTe-like phonons.¹⁷ Additional modes attributed to clustering or disorder have been reported in bulk $\text{CdTe}_{0.65}\text{Se}_{0.35}$.¹⁸

Time-domain experiments were performed using a mode-locked Ti:sapphire laser (Tsunami, Spectra Physics), operating at the repetition rate of 83 MHz, which emitted femtosecond pulses, tunable between 1.55 and 1.62 eV. This range

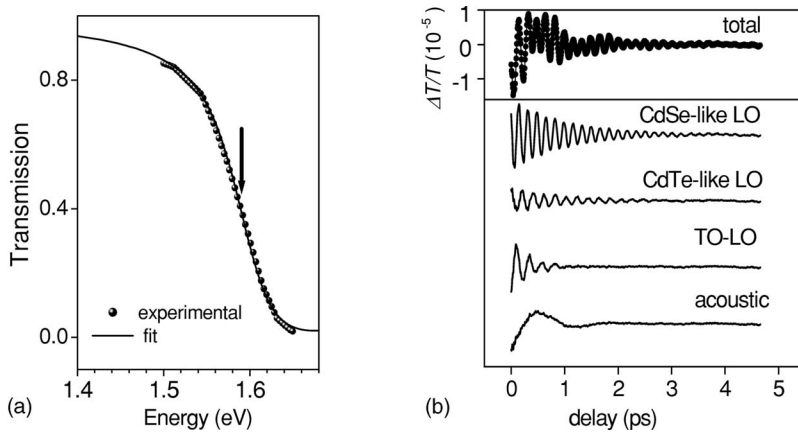


FIG. 1. (a) Transmission of the RG780 Schott filter near the main absorption edge. (b) Coherent phonons. The top trace shows the total differential transmission $\Delta T/T$ with the electronic background subtracted. The full circles are the experimental points; the line is the LP fit. The lower panel shows the individual phonon contributions, which add up to the total signal. From top to bottom, the frequencies of the modes are 197, 162, 140, and 24 cm^{-1} . The arrow in (a) indicates the laser central energy at which (b) was obtained.

covers the region of the main absorption edge of the sample; see Fig. 1(a). The average pump intensity was set at 2 kW/cm^2 and the probe intensity was six times lower. The polarizations of the pump and probe beams were perpendicular to each other to reduce the scattering of the pump into the detector. Special care was taken in keeping the pulse width nearly constant at about 45–50 fs. A detailed description of the setup for pump-probe measurements can be found in Ref. 14.

Raman measurements were performed with an XY Dilor Spectrometer. We excited the sample with a continuous wave home-made Ti:Sapphire laser, tunable between 1.53 and 1.72 eV, as well as with the 514 nm (2.41 eV) and 488 nm (2.54 eV) lines of an Ar^+ ion laser. To avoid sample heating, the light was focused with a cylindrical lens.

III. RESULTS AND DISCUSSION

Figure 1(b) shows the normalized differential transmission $\Delta T/T$ (T is the total probe transmission) as a function of the probe delay at the laser central energy $E_c = 1.587$ eV. The raw data show oscillations due to coherent phonons superimposed on an exponential background, arising from electronic excitations. For clarity, this electronic contribution was removed from the total signal. We fit our time domain data to expressions of the form

$$\sum_k A_k \exp(-\Gamma_k t) \sin(\Omega_k t + \phi_k) \quad (1)$$

using linear prediction (LP) methods.¹⁹ This procedure gives as output not only the amplitude A , phase ϕ , damping Γ , and frequency Ω of each mode, but also the total number of oscillators. Figure 1(b) shows an example of such a fit and, separately, the individual contributions of the various modes. Four modes can be distinguished; there are two LO modes at 197 and 162 cm^{-1} , one confined longitudinal acoustic (LA) mode at 24 cm^{-1} and a mixed TO-LO mode at 40 cm^{-1} . In this paper we concentrate only on acoustic modes. For a detailed discussion on optical modes, see Ref. 14.

Figure 2 shows the Raman spectrum recorded at 2.54 eV in a configuration where the incident and the scattered light have the same polarization. The laser energy is well above the main absorption edge. The single acoustic mode seen in

the time-domain measurements appears also in the Raman spectrum, but there are two additional modes at ~ 9 and ~ 15 cm^{-1} . We assign the acoustic oscillations in Fig. 1(b), of frequency ~ 24 cm^{-1} , and the RS peak at 32 cm^{-1} (Fig. 2) to the same confined acoustic phonon. The reason why the frequencies in both sets of data are different is explained below.

Following the work of Lamb²⁰ from the late 1800's, many authors have calculated the low-frequency spectrum of nanocrystallites, by approximating them as homogeneous elastic spheres.^{6,21,22} In actual experiments, the assignment of acoustic vibrations is always challenging and often unsupported. Because of this, there is considerable confusion in the literature as to the proper assignment of these modes. Matrix properties, the value of the transverse and longitudinal sound velocity in the nanocrystallites and material inhomogeneities are some of the factors that determine the acoustic frequencies and complicate the assignments. In a recent work, Savit *et al.*^{23,24} pointed out these difficulties, giving an extensive comparison among different theoretical approaches, and showing phonon shifts and the appearance of new modes due to the matrix. On the other hand, Raman selection rules for spherical particles are well established for excitation below

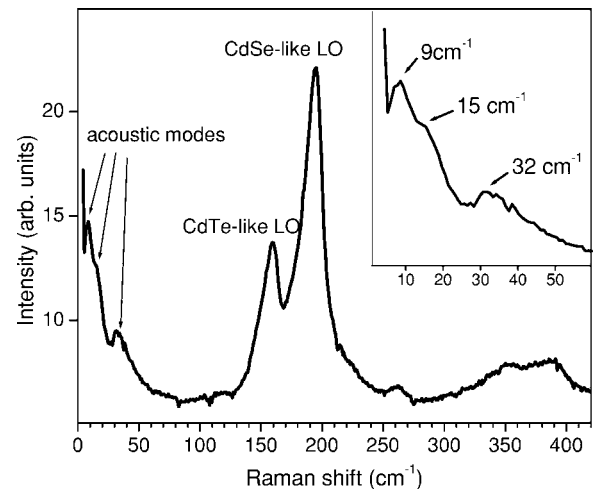


FIG. 2. Raman spectrum at room temperature using a 488 nm (2.54 eV) excitation line from an Ar^+ laser in the parallel configuration. The inset shows the low frequency acousticlike modes.

the gap,²⁵ whereas forbidden acoustic as well as optical modes are often observed in the absorptive region.²⁶

Acoustic vibrations are grouped into two categories, spheroidal and torsional. The latter involve only shear motions, which are Raman inactive,⁷ while the former encompasses both shear and stretching motions. The modes of a sphere are characterized by the integer n (which labels the sequence of eigenmodes in increasing order) and the spherical harmonic integers l and m ($\leq l$). The $l=0$ spheroidal mode is purely radial and fully symmetric. It has been shown that the Raman intensity for the so-called surface mode ($n=0$) is about ten times higher than for the first overtone ($n=1$).²¹ For transparent substances, only the $l=0$ and $l=2$ spheroidal modes are Raman active (however, see Ref. 21).²⁵

Independent of the boundary conditions, the acoustic phonon frequency is always proportional to the inverse radius²²

$$\Omega_{ln} = S_{ln} \frac{v}{2Rc}. \quad (2)$$

Here Ω_{ln} is given in cm^{-1} , the radius R in cm, and v is the sound velocity (longitudinal for $l=0$, transversal for $l=2$) expressed in the same units as the speed of light c . S_{ln} is a coefficient that depends on the ratio of the sound velocities, the choice of the boundary condition, the angular momentum l and the harmonic number n (note that the frequency does not depend on m). As the speed of sound in $\text{CdTe}_{1-x}\text{Se}_x$ is not known, we assume that $v_L/v_T \sim 2.3$, as for CdSe and CdTe.²¹ The coefficients S_{ln} we used were gained from Ref. 22. For fixed surface boundary conditions, $S_{00}=1.43$ and $S_{20}=2.07$. In the following, we label the acoustic modes according to their frequency.

Figure 3 shows the frequency of the coherent acoustic mode as a function of the laser excitation energy. Based on the previous discussion, we assign this vibration to the fully symmetric Ω_{00} confined mode. This assignment, and the fact that the pump-probe traces show only a single acoustic mode, is consistent with previous reports on acoustic phonon generation in rocksalt PbTe,²⁷ PbSe,¹⁶ and PbS,¹⁵ zincblende InAs (Ref. 28) and wurzite CdSe.²⁸ Notice that, for PbS, the Ω_{20} mode appears in the spontaneous Raman spectra, but not in the pump-probe traces.¹⁵ We further note that the differential transmission is given by²⁹

$$\Delta T \sim \left(\sum_{\gamma\mu} \Re_{\gamma\mu} E_{\gamma} E_{\mu} \right) \left(\sum_{\alpha\beta} \Re_{\alpha\beta} e_{\alpha} e_{\beta} \right), \quad (3)$$

where $\Re_{\gamma\mu}$ is the Raman tensor, E is the pump field, and e is the probe field. Hence, the standard pump-probe configuration allows the detection of fully-symmetric modes. It is important to emphasize that the experiments reported so far were all performed under resonant conditions where the acoustic phonon signal is enhanced.

Figure 3 clearly shows size-selective excitation behavior as the laser energy is moved across the absorption edge. The selectivity manifests itself as a shift of the acoustic phonon frequency. Higher laser energies resonantly excite smaller dots inside the distribution and, consequently, higher acoustic frequencies are detected. As shown by Eq. (2), the acoustic frequency is strongly dependent on the radius of the par-

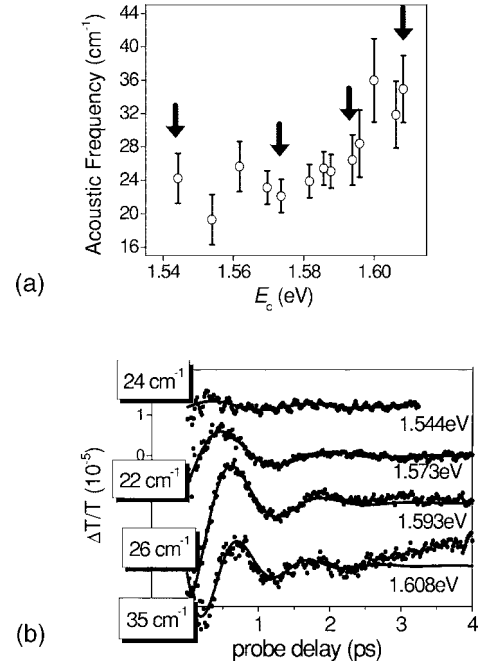


FIG. 3. Pump-probe results. (a) Acoustic frequency as a function of the laser central energy. The frequency moves upward as the laser selectively excites dots of smaller radii. Arrows indicate values corresponding to the four time-domain traces shown in (b).

ticle. This produces substantial changes in the traces even for small changes of the laser excitation energy. Previous studies reported similar size-selective excitation in spontaneous Raman measurements on CdS⁸ and pump-probe measurements in PbTe.²⁷

Raman spectra were obtained in the same range of excitation energies we used in the pump-probe measurements, and also for excitation well above the lowest-lying exciton. Figure 4 shows the low-frequency region of the Raman spectra. In the off-resonance case we observe a single broad peak, which we assign to the Ω_{20} mode. For nonresonant conditions and cubic lattice QDs, Montagna *et al.* showed that the $l=2$ mode is the only one that is Raman active.²¹ This is consistent with our data. The intensity of the higher-frequency mode at $\sim 32 \text{ cm}^{-1}$ increases as the laser energy moves into the resonant region. This is the Ω_{00} mode which dominates the pump-probe traces. Although it is resonantly enhanced, as in the time-domain data, the Ω_{00} Raman mode does not exhibit the size-selectivity shown by the time-domain experiments. Rather, its frequency seems to reflect the *average* radius of the QD distribution. The mode at $\sim 9 \text{ cm}^{-1}$ which appears well above the band gap (see Fig. 2) is assigned to the Raman-forbidden Ω_{10} vibration.

Tentatively, we attribute the different time vs frequency domain behavior of the Ω_{00} mode to the fact that double-resonant terms in the Raman matrix operate for pump-probe excitation, but not for spontaneous RS. This can be seen as follows. The most resonant term of the nonlinear polarizability associated with (spontaneous) Raman processes is of the form³⁰

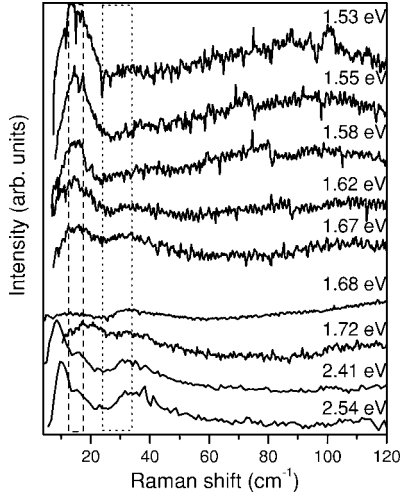


FIG. 4. Raman spectra at 300 K for various laser excitation energies. The low-frequency data show three different confined acoustic phonons. The region delimited by the dotted (dashed) lines defines the range of the Ω_{00} (Ω_{20}) acoustic mode expected for size-selective resonant excitation. The symmetric mode Ω_{00} at about 33 cm^{-1} is strongly resonant. The Ω_{20} mode is the only one seen in the non-absorbing regime. The lowest frequency mode at about 9 cm^{-1} is assigned to the Ω_{11} mode and can only be seen for excitation well above the band gap.

$$\mathbf{P}_{\omega-\Omega_R}^{\text{Raman}} \propto \frac{\mathbf{E}_\omega}{(\omega_R - i\gamma_R - \omega)(\omega_R - i\gamma_R - \omega + \Omega_R)}. \quad (4)$$

Here \mathbf{E}_ω is the laser electric field of frequency ω , ω_R (γ_R) is the exciton frequency (lifetime) for a dot of radius R and Ω_R is the acoustic phonon frequency. Incoming and outgoing resonances occur, respectively, when the energy of the incident and scattered photon coincide with the exciton energy and, for a given dot, it is apparent that the resonance occurs *either* in the incoming or outgoing channel but not in both. Similarly, for impulsive-stimulated RS the expression for the driving force F contains the resonant term³⁰

$$F \propto \frac{\mathbf{E}_\omega \mathbf{E}_{\omega-\Omega}^*}{(\omega_R - i\gamma_R - \omega)(\omega_R + i\gamma_R - \omega + \Omega_R)}. \quad (5)$$

Unlike spontaneous RS, however, both denominators in Eq. (5) can simultaneously vanish to give a *double resonance* since the spectrum of the laser pulse contains both incoming and outgoing frequencies. The reason why CdS (Ref. 8) but not $\text{CdTe}_{0.68}\text{Se}_{0.32}$ QDs exhibit size-selective RS excitation is not understood at this time.

Summarizing our results, Fig. 5 shows the measured dependence of the acoustic frequencies as a function of E_c . Using expressions that relate the exciton energy to the QD radius,³¹ the graph also shows the expected dependence on the QD radius, assuming size-selective excitation. The lines labeled Ω_{00} and Ω_{20} describe the radius dependence of the corresponding acoustic frequencies for a homogeneous distribution of QDs. Stars represent the Raman frequencies obtained with excitation well above the absorption edge. The measured values agree with the calculated Ω_{00} , Ω_{20} , and Ω_{10} frequencies for a QD radius equal to the average radius of

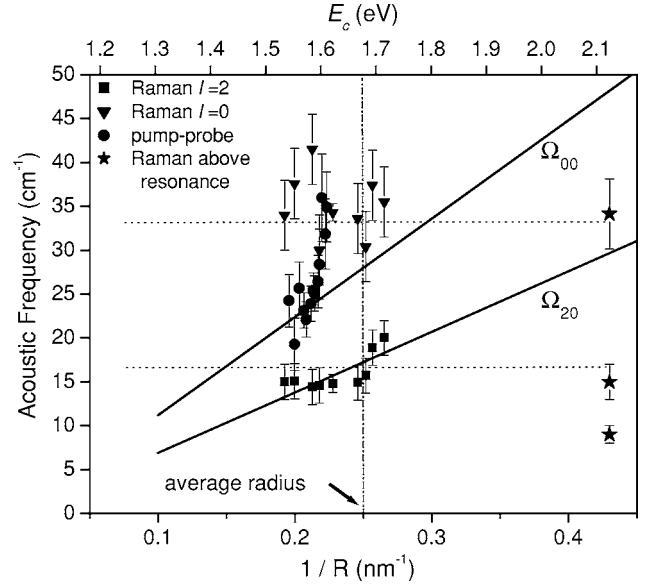


FIG. 5. Dependence of the acoustic frequencies on E_c and $1/R$ (see text). Full circles correspond to pump-probe and the other symbols to RS measurements. Lines represent calculated values for a homogeneous distribution of crystallites. The strong E_c dependence exhibited by the Ω_{00} mode in pump-probe experiments is attributed to size-selective excitation. RS measurements of the same mode (triangles) cluster around a value corresponding to the average radius of the distribution.

the distribution. The Ω_{00} frequency determined in pump-probe measurements varies in the expected manner with the resonantly selected radius, but the agreement between experiment and theory is rather poor. The Ω_{20} Raman mode appears to follow better the theoretical predictions but, because the expected shift is rather small, it is difficult to assert as to whether or not the observed shift is due only to size selection.

Consistent with the size-selection interpretation, as shown in Fig. 6, the Ω_{00} linewidth obtained in pump-probe increases from 3 cm^{-1} , at $1/R \sim 0.2$, to 8 cm^{-1} for $1/R \sim 0.22$. Also shown in Fig. 6 are linewidths obtained from

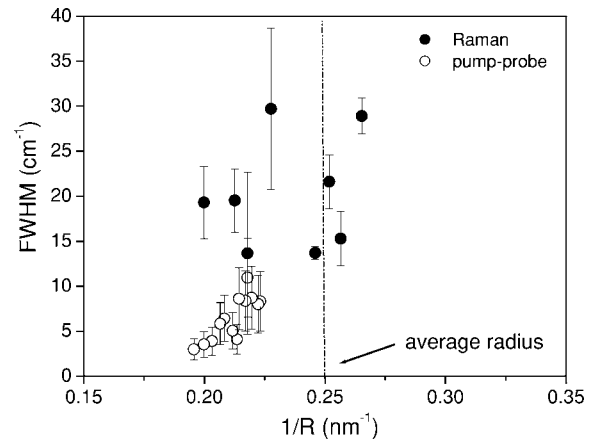


FIG. 6. Dependence of the full width half maximum (FWHM) on $1/R$ of the Ω_{00} mode, for both Raman and pump-probe measurements.

RS measurements which, in spite of the large error bars, seem to be always greater than the pump-probe linewidths. This fact supports the idea that the signal in pump-probe experiments originates from a much narrower distribution of QD sizes.

IV. CONCLUSIONS

Spontaneous RS measurements in $\text{CdTe}_{0.68}\text{Se}_{0.32}$ QDs reveal three acoustic-related peaks which were ascribed to the Ω_{00} , Ω_{20} and Ω_{10} modes. Ω_{00} is the only mode observed in pump-probe experiments, in a geometry which favors the detection of symmetric modes. The Ω_{00} mode exhibits size selectivity in pump-probe but not in spontaneous Raman measurements, even though the Ω_{00} cross section is strongly

enhanced at the gap (consistent with the fact that the associated Raman tensor is strictly zero for cubic lattices, this mode is not observed below the gap).²¹ The Raman signal is very weak outside the resonant range complicating the assignment of the peak frequencies and shifts. The enhancement of the pump-probe signal at the absorption edge is due in part to the large variation of the absorption in that region and also because of double-resonant behavior.

ACKNOWLEDGMENTS

Work supported by the AFOSR under Contract No. F49620-00-1-0328 through the MURI program. One of us (A.V.B.) acknowledges partial support from CONICET, Argentina.

*Electronic address: bragas@df.uba.ar

†Present address: Institut des Nanosciences de Paris, UMR 7588, CNRS/Université Paris VI et VII, Campus Boucicaud, 140 rue de Lourmel, 75015 Paris, France and Department of Physics, King's College London, Strand, London WC2R 2LS, United Kingdom.

¹X. Michalet, F. Pinaud, T. D. Lacoste, M. Dahan, M. P. Bruchez, A. P. Alivisatos, and S. Weiss, *Single Mol.* **2**, 261 (2001).

²T. M. Jovin, *Nat. Struct. Biol.* **1**, 32 (2003).

³V. Spagnolo, G. Scamarcio, M. Lugará, and G. C. Righini, *Superlattices Microstruct.* **16**, 51 (1994).

⁴T. Bischof, M. Ivanda, G. Lermann, A. Materny, W. Kiefer, and J. Kalus, *J. Raman Spectrosc.* **27**, 297 (1996).

⁵W. S. O. Rodden, C. M. S. Torres, and C. N. Ironside, *Semicond. Sci. Technol.* **10**, 807 (1995).

⁶P. Verma, W. Cordts, G. Irmer, and J. Monecke, *Phys. Rev. B* **60**, 5778 (1999).

⁷A. Roy and A. K. Sood, *Solid State Commun.* **97**, 97 (1996).

⁸L. Saviot, B. Champagnon, E. Duval, and A. I. Ekimov, *Phys. Rev. B* **57**, 341 (1998).

⁹P. Verma, L. Gupta, S. C. Abbi, and K. P. Jain, *J. Appl. Phys.* **88**, 4109 (2000).

¹⁰P. Verma, L. Gupta, S. C. Abbi, and K. P. Jain, *J. Appl. Phys.* **88**, 4109 (2000).

¹¹Y. N. Hwang, S. H. Park, and D. Kim, *Phys. Rev. B* **59**, 7285 (1999).

¹²A. Ingale and K. C. Rustagi, *Phys. Rev. B* **58**, 7197 (1998).

¹³M. I. Vasilevskiy, A. G. Rolo, M. J. M. Gomes, O. V. Vikhrova, and C. Ricolleau, *J. Phys. A* **13**, 3491 (2001).

¹⁴A. V. Bragas, C. Aku-Leh, S. Costantino, A. Ingale, J. Zhao, and R. Merlin, *Phys. Rev. B* **69**, 205306 (2004).

¹⁵T. D. Krauss and F. W. Wise, *Phys. Rev. Lett.* **79**, 5102 (1997).

¹⁶M. Ikezawa, T. Okuno, Y. Masumoto, and A. A. Lipovskii, *Phys. Rev. B* **64**, 201315(R) (2001).

¹⁷Z. C. Feng, P. Becla, L. S. Kim, S. Perkowitz, Y. P. Feng, H. C. Poon, K. P. Williams, and G. D. Pitt, *J. Cryst. Growth* **138**, 239 (1994).

¹⁸S. Perkowitz, and L. S. Kim, and P. Becla, *Phys. Rev. B* **43**, 6598 (1991).

¹⁹H. Barkhuijsen, R. De Beer, W. M. M. J. Bovée, and D. Van Ormondt, *J. Magn. Reson.* (1969-1992) **61**, 465 (1985).

²⁰H. Lamb, *Proc. London Math. Soc.* **13**, 187 (1882).

²¹M. Montagna and R. Dusi, *Phys. Rev. B* **52**, 10080 (1995).

²²L. Saviot, B. Champagnon, E. Duval, I. A. Kudriavtsev, and A. I. Ekimov, *J. Non-Cryst. Solids* **197**, 238 (1996).

²³L. Saviot, D. B. Murray, and M. C. Marco de Lucas, *Phys. Rev. B* **69**, 113402 (2004).

²⁴L. Saviot and D. B. Murray, *Phys. Rev. Lett.* **93**, 055506 (2004).

²⁵E. Duval, *Phys. Rev. B* **46**, 5795 (1992).

²⁶M. P. Chamberlain, C. Trallero-Giner, and M. Cardona, *Phys. Rev. B* **51**, 1680 (1995).

²⁷E. R. Thoen, G. Steinmeyer, P. Langlois, E. P. Ippen, G. E. Tudury, C. H. Brito Cruz, L. C. Barbosa, and C. L. Cesar, *Appl. Phys. Lett.* **73**, 2149 (1998).

²⁸G. Cerullo, S. De Silvestri, U. Banin, *Phys. Rev. B* **60**, 1928 (1999).

²⁹R. Merlin, *Solid State Commun.* **102**, 207 (1997).

³⁰T. E. Stevens, J. Kuhl, and R. Merlin, *Phys. Rev. B* **65**, 144304 (2002).

³¹M. I. Vasilevskii, E. I. Akinkina, A. M. de Paula, and E. V. Anda, *Semiconductors* **32**, 1229 (1998).